

Local Measurement Based Robust Voltage Stability Index & Identification of Voltage Collapse Onset

Kishan Guddanti, *Student Member, IEEE*, Amarsagar Matavalam, *Member, IEEE*, Yang Weng, *Member, IEEE*

Abstract—This paper addresses the problem of real-time monitoring of long-term voltage instability (LTVI) by using local field measurements. Existing local measurement-based methods use Thevenin equivalent parameter estimation that is sensitive to the noise in measurements. For solving this issue, we avoid the Thevenin approach by projecting the power flow equations as circles to develop local static-voltage stability indicator (LS-VSI) that is robust to measurement noises. The proposed method is an attractive option for practical implementation because of its decentralized nature, robustness to noise, and realistic modeling. Next, we utilize LS-VSI to propose a new local dynamic - VSI (LD-VSI) to identify the LTVI triggered by large disturbances and load tap changer dynamics. LD-VSI can identify not only the onset of instability with an alarm but also the voltage collapse point (VCP). Extensive numerical validation comparing LS-VSI with existing methods is presented on IEEE 30-bus and larger test systems like 2000-bus Texas synthetic grid to validate the robustness, accuracy, and situational awareness feature. We also verify the LD-VSI behavior on the Nordic power grid using PSSE dynamic simulation. When compared to existing methods, we observe that LD-VSI is not only more robust to measurement noise but also can identify VCP.

I. INTRODUCTION

Long-term voltage instability (LTVI) is a quasi-static bifurcation (nose point of the PV curve) [1], if left unattended, LTVI results in a system-wide voltage collapse and blackout [1]. Using field measurements, one can compute the margin (a measure of distance) from the current operating condition to LTVI. This measure of distance is quantified using metrics known as voltage collapse proximity indices (VCPIs). Based on the telecommunication requirement between the field measurement devices and control center, online monitoring of LTVI can be classified majorly into (a) wide-area VCPIs [2], [3] and (b) local VCPIs [4]–[8]. Both approaches, wide-area and local, have a set of advantages and disadvantages which are well documented in [9]. The online monitoring tools aim to aid the emergency control actions using system protection schemes (SPSs). Different online monitoring tools provide different types of output information that are used to trigger the SPSs. Based on the monitoring system type used [10], SPSs are classified as wide-area SPSs (uses the output of wide-area VCPIs to trigger SPS) and local SPSs (uses the output of local VCPIs to trigger SPS).

A local SPS uses the output information from a local monitoring-type VCPI [4], [5], [7]. Local VCPIs calculate the two bus Thevenin equivalent [4], [5], [7] using real-time measurements at the bus of interest assuming *constant power loads* [6], [11]. However, [6], [12]–[14] showed that voltage stability is impacted by the load characteristics (ZIP load models), and the assumption of constant power loads is not accurate depending on the mechanism of the instability event. Hence, the local VCPIs face two issues 1) the estimates of local VCPIs for LTVI margin, derived for a two-bus

system assuming a constant power load, maybe pessimistic and inaccurate for the systems with mixed load types; 2) local VCPIs are highly impacted by the noise in measurements [8].

LS-VSI for small disturbance LTVI: In this work, we propose a new local VCPI known as “Local Static - Voltage Stability Indicator” (LS-VSI) that addresses the issues of 1) voltage-sensitive loads and 2) Thevenin equivalent parameters estimation (in the presence of noisy field measurements) by 1) incorporating the ZIP load dynamics into the LS-VSI formulation and 2) discarding the idea of obtaining two-bus Thevenin equivalent at the bus of interest, respectively.

Additionally, there is a different class of research focused on large disturbance long-term voltage stability phenomenon [15], [16]. This phenomenon considers the impact and interactions of nonlinear response due to devices such as motors, LTCs, generator field current limiters (OELs), and load restorative mechanisms (dynamic simulations). In case of a large disturbance phenomenon, [17] designed a local VCPI to output information (formula combining tap ratios of LTCs and voltages) which can be used to trigger SPSs. [17] showed that even though a voltage level-based VCPI is often a good indicator but it is not sufficient to provide a reliable, preventive picture of system security margins [17]. However, the methodology in [17] could not be extended to the buses without LTCs. [18] addressed the shortcomings of [17] by replacing the concept of LTCs with load conductance but its output is heavily impacted by the noise in measurement data as it uses a “filter” (moving average over large time windows) as a preprocessor. For example, selecting a good threshold for the length of the filter’s time window is a challenge. *It can either trigger false alarms or delay the identification of the event or completely miss the occurrence of an event that recovered in a short period.*

LD-VSI for large disturbance LTVI: In this work, we propose a second local-type VCPI for dynamic events arising from large disturbances. This proposed VCPI is known as “Local dynamic - VSI (LD-VSI)” and it can be used to trigger an alarm indicating the onset of a voltage emergency situation. We addressed the shortcomings of [17] and [18], by 1) designing the LD-VSI to be adaptable to any bus of interest and by 2) making LD-VSI less sensitive to the choice of the filter’s window size, respectively.

Both LS-VSI and LD-VSI are local measurement-based methods. For example, to monitor the LTVI phenomenon at bus 3 for the system in Fig. 1, using the LS-VSI and LD-VSI, we only need one measurement device at local bus 3 to collect the bus 3’s voltage phasor and adjacent lines’ current phasor measurements (local measurements).

Contributions of LS-VSI and LD-VSI:

- 1) LS-VSI incorporates the voltage-sensitive loads without constant power assumption like in [6], [11], [19].

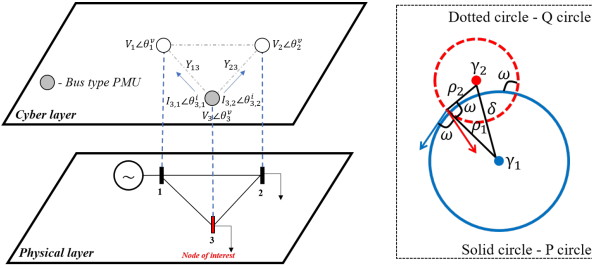
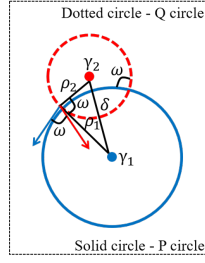


Fig. 1: Decentralized/local monitoring architecture of grid.

Fig. 2: Power flow circles (6) at bus d .



- 2) LS-VSI is more robust to measurement noise than other Thevenin-based [5] local monitoring schemes.
- 3) LD-VSI can be implemented at any load bus unlike the method in [17].
- 4) LD-VSI is less sensitive to the choice of filter's window size unlike NLI from [18]. Thus avoids false alarms and delayed event identification.
- 5) Unlike the methods in [17], [18], LD-VSI can identify (tends to minus infinity) the voltage collapse point (VCP).
- 6) NLI [18] cannot be computed when the load conductance (G) decreases as it discards such data. LD-VSI does not have such an assumption and thus, it can be used to continuously monitor the grid regardless of G value.

The paper is organized as follows: Section II demonstrates the impact of voltage-sensitive loads on voltage stability limit. Section III derives the local static - VSI (LS-VSI) considering the ZIP load models, LTCs and presents the algorithm that uses LS-VSI to study LTVI. Section V presents the numerical validation and comparison of LS-VSI with other methods in the literature. Section IV derives the local dynamic - VSI (LD-VSI) and presents the algorithm to use LD-VSI for LTVI studies. Section VI presents the numerical validation and comparison of LD-VSI with other methods in the literature. Section VII concludes the paper.

II. IMPACT OF VOLTAGE-SENSITIVE LOADS ON VOLTAGE STABILITY LIMIT

It is known that the saddle-node bifurcation point (SNBP i.e., voltage collapse point) occurs at the nose point (maximum power transfer point) of the PV curve. However, this is not valid in the case of a power system with ZIP loads [1]. In this section, with the help of three bus example, as shown in Fig. 4, we show that the SNBP may not always occur at the nose point where maximum power transfer occurs.

Let us consider a three bus fully connected mesh network with a slack bus at bus 1, two ZIP loads at buses 2 and 3. Branch impedance of lines connecting buses 1 to 3 and 2 to 3 is $0.0074 + j \cdot 0.0372$ p.u. and the impedance of line connecting buses 1 to 2 is $0.01 + j \cdot 0.05$ p.u. The loads located at buses 2 and 3 are represented by ZIP load model whose Z, I, and P coefficients are $\alpha_p = 0.8$, $\beta_p = 0$, and $\gamma_p = 0.2$ respectively. The real power at bus 2 (P_2) is given by

$$P_2 = P_b \cdot \lambda [\alpha_p \cdot \|\bar{V}_2\|^2 + \beta_p \cdot \|\bar{V}_2\| + \gamma_p], \quad (1)$$

where P_b , \bar{V}_2 , and λ are the nominal load power, voltage phasor at bus 2, and load scaling factor (continuation parameter in CPF-MATPOWER [20]) respectively. As shown in Fig. 3,

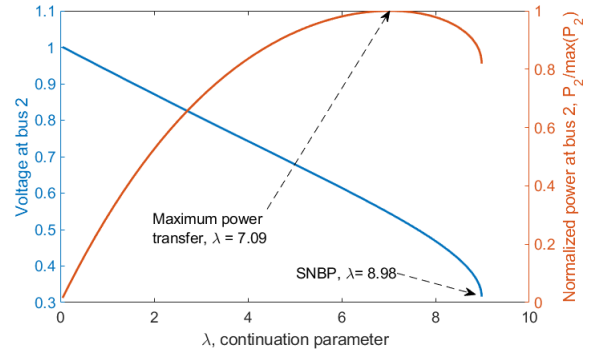


Fig. 3: Load scaling parameter (λ , continuation parameter) versus voltage at bus 2 when the load model is ZIP.

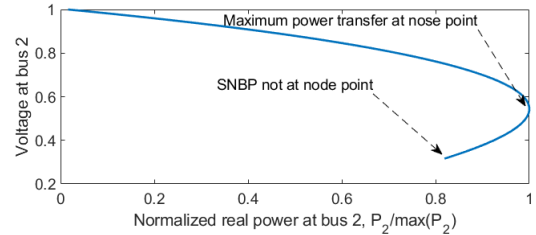


Fig. 4: PV curve at bus 2 when the load model is ZIP.

continuation power flow from MATPOWER is used to estimate the voltage at bus 2 while increasing the load demand ($P_b \cdot \lambda$) at buses 2 and 3 by increasing the λ . From Fig. 3, it can be observed that when $\lambda > 8.98$, the three bus system no longer has a power flow solution indicating the SNBP.

In addition, it can be observed from Fig. 3 that the power at bus 2 (P_2) is maximum when the load scaling factor (λ) is 7.09 but it is not maximum at the SNBP ($\lambda = 8.98$). This is because from (1), when load scaling factor (λ) increases the power injection at bus 2 (P_2) increases. However, as the loading ($P_b \cdot \lambda$) on the grid increases the voltage \bar{V}_2 decreases. At sufficiently large loading on the grid (in this example when $\lambda = 7.09$), the decrease in the magnitude of \bar{V}_2 (impedance nature of the load) dominates and reduces the net power injection at bus 2 (P_2). Fig. 4 shows the PV-curve demonstrating this phenomenon of SNBP not occurring at the maximum power transfer point (nose point of PV curve) when the power grid has ZIP loads. Additionally, as described in the latest 2020 task force report on test systems for voltage stability [21], *other important parameters of interest that can onset a voltage instability phenomenon are the combined operation of load tap changers (LTCs) and over excitation limiters (OELs)*. [17], [21] demonstrates this phenomenon in a dynamic simulation environment to incorporate device (LTCs, OELs, etc.) induced stability mechanisms. **Hence it is important to consider the impact of not only ZIP load models but also the LTCs device mechanics in online measurement-based monitoring applications of voltage stability.**

III. DERIVATION OF LS-VSI

In this section, we derive a new VCPI that requires only local measurements (decentralized) obtained from a single measurement device (located at the bus of concern) known as a local static voltage stability indicator (LS-VSI). This indicator will consider critical parameters such as ZIP loads and LTCs while determining the distance to voltage collapse.

First, we propose a new set of power flow equations that can incorporate critical parameters like the ZIP load model and load tap changers (LTCs). Second, we recast the derived power flow equations with detailed modeling of ZIP loads and LTCs into a decentralized/local framework. Finally, use these new equations to derive the proposed decentralized/local LS-VSI.

A. Power Flow Equations with ZIP loads and LTCs

Let p_d and q_d be the active and reactive power injections at bus d . Let $\bar{Y}_{d,k} = g_{d,k} + j \cdot b_{d,k}$ be the $(d, k)^{th}$ element of the admittance matrix Y . Let $v_{d,r}$ and $v_{d,i}$ be the real and imaginary parts of the voltage phasor (\bar{V}_d) at bus d , respectively. We represent bus d 's neighboring bus set as $\mathcal{N}(d)$. In the following subsections, LTCs and ZIP load model incorporated power flow equations in rectangular voltage coordinate are derived. *In the interest of space, the derivation steps are not included in the initial submission.*

1) Load Tap Changers and Shunts

As shown in Fig. 5, let us consider an LTC connecting buses d and f , buses d and f are on non-tap and tap side of the LTC respectively. \bar{Y}_{df} be its short circuit admittance, $\bar{Y}_d^{Sh} = g_d^{Sh} + j \cdot b_d^{Sh}$ and $\bar{Y}_f^{Sh} = g_f^{Sh} + j \cdot b_f^{Sh}$ are the shunt admittances at buses d and f respectively. The π equivalent representation of the LTC with shunts is presented in Fig. 5 on the right hand side.

$\bar{Y}_d^p = g_d^p + j \cdot b_d^p = \bar{Y}_{df} \cdot (a - 1)/a$, and $\bar{Y}_f^p = g_f^p + j \cdot b_f^p = \bar{Y}_{df} \cdot (1 - a)/a^2$ represent the shunt equivalents of LTC on non-tap and tap side respectively. The neighboring bus set of bus d is $\mathcal{N}(d) = \{f\}$. The conjugate operation is denoted by $(\cdot)^*$. The net apparent power injection at bus d is given by

$$\begin{aligned} \bar{S}_d &= \bar{V}_d \cdot \left(\sum_{k \in \mathcal{N}(d)} \bar{Y}_{d,k} \cdot \bar{V}_{dk} + \bar{Y}_d^p \cdot \bar{V}_d + \bar{Y}_d^{Sh} \cdot \bar{V}_d \right)^* \\ &= \bar{V}_d \cdot \left(\sum_{k \in \mathcal{N}(d)} \bar{Y}_{d,k} \cdot \bar{V}_{dk} \right)^* + \bar{V}_d \cdot \bar{V}_d^* \cdot (\bar{Y}_d^{p*} + \bar{Y}_d^{Sh*}), \\ &= \bar{V}_d \cdot \left(\sum_{k \in \mathcal{N}(d)} \bar{Y}_{d,k} \cdot \bar{V}_{dk} \right)^* + (v_{d,r}^2 + v_{d,i}^2) \cdot \\ &\quad (g_d^p + g_d^{Sh} - j \cdot (b_d^p + b_d^{Sh})). \end{aligned}$$

Let $\bar{S}_d = p_d + j \cdot q_d$ and upon further simplification, we get the new power flow equations in rectangular voltage coordinates considering both the LTCs and shunts as shown below.

$$p_d = w_{d,1} \cdot v_{d,r}^2 + w_{d,2} \cdot v_{d,r} + w_{d,1} \cdot v_{d,i}^2 + w_{d,3} \cdot v_{d,i}, \quad (2a)$$

$$q_d = w_{d,4} \cdot v_{d,r}^2 - w_{d,3} \cdot v_{d,r} + w_{d,4} \cdot v_{d,i}^2 + w_{d,2} \cdot v_{d,i}. \quad (2b)$$

The parameters $w_{d,1}$, $w_{d,2}$, $w_{d,3}$ and $w_{d,4}$, considering the LTCs and shunts are given by

$$\begin{aligned} w_{d,1} &= - \sum_{k \in \mathcal{N}(d)} g_{d,k} + g_d^p + g_d^{Sh}, w_{d,4} = \sum_{k \in \mathcal{N}(d)} b_{d,k} - b_d^p \\ &\quad - b_d^{Sh} \end{aligned} \quad (3a)$$

$$\begin{aligned} w_{d,2} &= \sum_{k \in \mathcal{N}(d)} (v_{k,r} g_{d,k} - v_{k,i} b_{d,k}), w_{d,3} = \sum_{k \in \mathcal{N}(d)} (v_{k,r} b_{d,k} \\ &\quad + v_{k,i} g_{d,k}). \end{aligned} \quad (3b)$$

(2) is modified to include the ZIP load model as shown below.

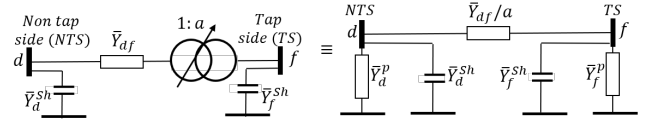


Fig. 5: π equivalent of load tap changing transformer.

2) ZIP Load Models

The real and reactive power demand at a bus d with ZIP load model is given by

$$p_d = p_L \cdot [\alpha_p \cdot \|\bar{V}\|^2 + \beta_p \cdot \|\bar{V}\| + \gamma_p], \quad (4a)$$

$$q_d = q_L \cdot [\alpha_q \cdot \|\bar{V}\|^2 + \beta_q \cdot \|\bar{V}\| + \gamma_q], \quad (4b)$$

where p_L , q_L are the nominal real and reactive powers of the load respectively. \bar{V} is the normalized voltage phasor. p_d , q_d are the net real and reactive power injections at bus d with a ZIP load. α_p , β_p , γ_p are the Z, I, P coefficients of real power respectively and α_q , β_q , γ_q are the Z, I, P coefficients of reactive power respectively. (2) is further modified to include ZIP load model as show below

$$\begin{aligned} p_d &= w_{d,1} \cdot v_{d,r}^2 + w_{d,2} \cdot v_{d,r} + w_{d,1} \cdot v_{d,i}^2 + w_{d,3} \cdot v_{d,i}, \\ &\implies p_L \cdot [\alpha_p \cdot \|\bar{V}\|^2 + \beta_p \cdot \|\bar{V}\| + \gamma_p] = w_{d,1} \cdot v_{d,r}^2 + \\ &\quad w_{d,2} \cdot v_{d,r} + w_{d,1} \cdot v_{d,i}^2 + w_{d,3} \cdot v_{d,i}, \\ &\implies p_L \cdot [\alpha_p \cdot (v_{d,r}^2 + v_{d,i}^2) + \beta_p \cdot (v_{d,r}^2 + v_{d,i}^2)^{0.5} + \gamma_p] = \\ &\quad w_{d,1} \cdot v_{d,r}^2 + w_{d,2} \cdot v_{d,r} + w_{d,1} \cdot v_{d,i}^2 + w_{d,3} \cdot v_{d,i}. \end{aligned} \quad (5)$$

To obtain the circle representing formulation, the power flow equations must be in the form of a homogeneous quadratic equation. However, the real power equation (5) does not appear as a circle by physical law when there is a constant current components $\beta_p, \beta_q \neq 0$. We identify this condition ($\beta_p \neq 0$, and $\beta_q \neq 0$) as a degenerate condition where the power flow equations by physical law cannot be represented as circles anymore. In this section, we propose a formulation for the ZIP load models whose constant current component is zero i.e., $\beta_p = 0$, and $\beta_q = 0$. *In the interest of space, we omitted our solution for degenerate conditions in this initial submission.*

When $\beta_p = 0$, and $\beta_q = 0$, the real power equation in (6a) is obtained by rearranging the terms in (5). A similar approach is carried out to obtain the reactive power equation as well. They are as follows

$$p_L \cdot \gamma_p = h_{d,1} \cdot v_{d,r}^2 + h_{d,2} \cdot v_{d,r} + h_{d,1} \cdot v_{d,i}^2 + h_{d,3} \cdot v_{d,i}, \quad (6a)$$

$$q_L \cdot \gamma_q = h_{d,4} \cdot v_{d,r}^2 - h_{d,3} \cdot v_{d,r} + h_{d,4} \cdot v_{d,i}^2 + h_{d,2} \cdot v_{d,i}. \quad (6b)$$

The parameters $h_{d,1}$, $h_{d,2}$, $h_{d,3}$ and $h_{d,4}$, considering the ZIP load model, LTCs and shunts are given by

$$\begin{aligned} h_{d,1} &= - \sum_{k \in \mathcal{N}(d)} g_{d,k} + g_d^p + g_d^{Sh} - p_L \cdot \alpha_p, h_{d,4} = \sum_{k \in \mathcal{N}(d)} b_{d,k} \\ &\quad - b_d^p - b_d^{Sh} - q_L \cdot \alpha_q \end{aligned} \quad (7a)$$

$$\begin{aligned} h_{d,2} &= \sum_{k \in \mathcal{N}(d)} (v_{k,r} g_{d,k} - v_{k,i} b_{d,k}), h_{d,3} = \sum_{k \in \mathcal{N}(d)} (v_{k,r} b_{d,k} \\ &\quad + v_{k,i} g_{d,k}). \end{aligned} \quad (7b)$$

Equation (6) represents the final representation of power flow equations with ZIP load models and LTCs. Using this representation, we derive the proposed local VCPI for small disturbance analysis (LS-VSI) in the subsection below.

B. Derivation of Local Static - Voltage Stability Indicator

In this section, we will first design the measurement-based local monitoring scheme using (6). We eliminate the neighboring bus voltages $\bar{V}_k = v_{k,r} + j \cdot v_{k,i}$ in (6) by using the branch currents as shown in (8).

$$\bar{V}_k = \bar{V}_{d,m} - I_{d,k} \cdot Z_{d,k}, \quad \forall k \in \mathcal{N}(d), \quad (8)$$

where $I_{d,k}$ is the branch current phasor measurement, $\bar{V}_{d,m}$ is the voltage phasor measurement at bus d and $Z_{d,k}$ is the complex impedance of adjacent branch of bus d connecting bus k . Substituting (8) in (6), the proposed decentralized/local power flow equations are given by (6) where its new updated parameters $h_{d,1}$, $h_{d,2}$, $h_{d,3}$, & $h_{d,4}$ are shown below in (9).

$$h_{d,1} = \sum_{k \in \mathcal{N}(d)} -g_{d,k} - g_d^p - g_d^{Sh} + p_L \cdot \alpha_p, \quad h_{d,4} = \sum_{k \in \mathcal{N}(d)} b_{d,k} - b_d^p - b_d^{Sh} - q_L \cdot \alpha_q \quad (9a)$$

$$h_{d,2} = \sum_{k \in \mathcal{N}(d)} (\Re\{\bar{V}_{d,m} - I_{d,k} \cdot Z_{d,k}\} g_{d,k} - \Im\{\bar{V}_{d,m} - I_{d,k} \cdot Z_{d,k}\} b_{d,k}), \quad (9b)$$

$$h_{d,3} = \sum_{k \in \mathcal{N}(d)} (\Re\{\bar{V}_{d,m} - I_{d,k} \cdot Z_{d,k}\} b_{d,k} + \Im\{\bar{V}_{d,m} - I_{d,k} \cdot Z_{d,k}\} g_{d,k}). \quad (9c)$$

We call the power flow equations in (6) with new updated parameters ($h_{d,1}$, $h_{d,2}$, $h_{d,3}$, & $h_{d,4}$) from (9) as decentralized/local because these transformed power flow equations are now in terms of measurements from a single measurement device located at the bus of interest d . A further explanation is given below:

- 1) The measurement device located at bus d can provide the measurements of voltage phasor measurement at bus d ($\bar{V}_{d,m}$) and adjacent branches' current measurements connected to bus d ($\bar{I}_{d,k} \forall k \in \mathcal{N}(d)$) **as the system operating condition changes with time.**
- 2) Using these measurements ($\bar{V}_{d,m}$, $\bar{I}_{d,k}$), the parameters ($h_{d,1}$, $h_{d,2}$, $h_{d,3}$, & $h_{d,4}$) from (9) can be computed instantaneously and **tracked in real-time.**
- 3) **Please note that we do not assume that the field measurements ($\bar{V}_{d,m}$, $\bar{I}_{d,k}$) are constant but rather when the system operating condition changes (different loading snapshots) then the field measurement device located at bus d will automatically provide the real-world measurements reflecting the changes in the system operating conditions. The proposed method tracks the system state using the field measurements in real-time. This is standard and followed by every measurement-based monitoring method in the literature [5]–[7].**
- 4) Finally, **at a snapshot**, given the local field measurements ($\bar{V}_{d,m}$, $\bar{I}_{d,k}$) at bus d , the parameters ($h_{d,1}$, $h_{d,2}$, $h_{d,3}$, & $h_{d,4}$) from (9) are calculated and hence, (6) represents a homogeneous quadratic equations (circles) in the domain of $v_{d,r}$ and $v_{d,i}$.

As described in point (4) above, at a given snapshot, power flow equations in (6) can be visualized as power flow circles. [8] shows that when the power system experiences voltage

collapse then the distance between the power flow circles is zero (internally or externally touching circles). As shown in Fig. 2, to derive the proposed LS-VSI, we use the law of cosines in the triangle formed by the centers of the power flow circles and their points of intersections to identify the distance to voltage collapse. From Fig. 2, let the centers of the real and reactive power circles be γ_1 and γ_2 respectively. Let the radius of real and reactive power circles be ρ_1 and ρ_2 respectively. The distance between the centers of the power flow circles is given by δ i.e., $\|\gamma_1 - \gamma_2\|_2 = \delta$. The parameters (γ_1 , γ_2 , ρ_1 , and ρ_2) are obtained from (9). As shown in Fig. 2, using the cosine rule, we get $\cos^2(\omega) = \frac{\beta_{12}^2}{\rho_1^2 \cdot \rho_2^2}$ where $\beta_{12} = \frac{\delta^2 - (\rho_1^2 + \rho_2^2)}{2}$, and ω is the angle between the radii of real and reactive power circles. **When the real and reactive power circles touch each other either externally or internally, it results in the voltage collapse i.e., SNBP, this background is presented in [1], [8].** In this paper, we use the property of $\cos^2(\omega) \leq 1$, with equality occurring at the SNBP. Upon further simplification, we obtain the proposed LS-VSI as shown in (11). The results of the proposed decentralized index can be interpreted by understanding its lower bound. When the power flow circles touch each other i.e., $\delta = \rho_1 \pm \rho_2$, the proposed LS-VSI becomes zero i.e., $\Pi_1 = 0$ indicating the SNBP.

$$\begin{aligned} \cos^2(\omega) \leq 1, & \implies \rho_1^2 \cdot \rho_2^2 - \beta_{12}^2 \geq 0, & (10) \\ \implies & \frac{(h_{d,2}^2 + h_{d,3}^2)}{8 \cdot h_{d,1}^2} + \frac{(h_{d,2}^2 + h_{d,3}^2)}{8 \cdot h_{d,4}^2} + \frac{0.5p}{h_{d,1}} + \frac{0.5q}{h_{d,4}} + \\ & \left(\frac{(h_{d,2}^2 + h_{d,3}^2)}{4 * h_{d,1}^2} + \frac{p_L \cdot \gamma_p}{h_{d,1}} \right) \cdot \left(\frac{(h_{d,2}^2 + h_{d,3}^2)}{4 * h_{d,4}^2} + \frac{q_L \cdot \gamma_q}{h_{d,4}} \right) \\ & - 0.5 \left| \frac{h_{d,2}}{2h_{d,1}} + \frac{h_{d,3}}{2h_{d,4}} \right|^2 - 0.5 \left| \frac{h_{d,3}}{2h_{d,1}} - \frac{h_{d,2}}{2h_{d,4}} \right|^2 \geq 0. \\ \therefore \text{Proposed LS-VSI} = \Pi_1 & \geq 0. & (11) \end{aligned}$$

Here, we propose an algorithm for local (decentralized) measurement-based long-term voltage stability monitoring. The algorithm to monitor the voltage stability of the power grid is presented in Algorithm 1. **It is important to note that when (11) is equal to zero, it represents the SNBP (voltage collapse) but not the nose point (maximum power point) of the PV curve as discussed in Section II.** Since step 1 to step 4 in Algorithm 1 are analytical equations, they can be computed nearly instantly with time complexity of $O(1)$, making it an attractive tool for online voltage stability assessment.

Algorithm 1 Local monitoring of SNBP at a given snapshot

Input : Measurements: \bar{V}_d , $I_{d,k}$, $Y_{d,k} \forall k \in \mathcal{N}(d)$, α_p , β_p , γ_p and α_q , β_q , γ_q at bus d .

Output: Proposed index (LS-VSI) at bus d .

- 1: Calculate the net injection at bus d i.e., $\bar{S}_d = p_d + j \cdot q_d$;
 - 2: Calculate the p_L and q_L using (4);
 - 3: Calculate parameters $h_{d,1}$, $h_{d,2}$, $h_{d,3}$ and $h_{d,4}$ using (9);
 - 4: **return** Calculate the proposed LS-VSI (Π_1) using (11).
-

IV. ALGORITHM 2 USING LD-VSI: LOCAL MEASUREMENT BASED MONITORING FOR LARGE DISTURBANCE LONG-TERM VOLTAGE STABILITY

In Section III, we proposed a decentralized algorithm to monitor LTVI for small disturbance phenomenon and its advantageous features are discussed in Section V. In this section, we propose another local (decentralized) measurement based algorithm for long-term voltage stability monitoring but for a large disturbance phenomenon. Large disturbance phenomenon corresponds to impact and interaction of nonlinear response of devices such as transformer tap changers (LTCs), generator field current limiters (OELs), and load restorative mechanisms [15], [16]. We use the benchmark IEEE Nordic test system presented in the 2020 Task Force report for voltage stability studies [21] to monitor the instability due to large disturbance phenomenon.

A. Large disturbance long-term voltage instability phenomenon in IEEE Nordic test system

Fig. 6 shows the IEEE Nordic test system. Detailed IEEE Nordic test system data, as well as operating points and responses of this system to contingencies, are provided in [21] and all relevant files are downloadable from the PSDP Committee web page [22]. Generators are modeled in detail including magnetic saturation, AVRs, and prime movers/governors. Active loads have both constant impedance ($\alpha_p = 0.5$) and power ($\gamma_p = 0.5$) components while the reactive loads have only constant impedance ($\alpha_q = 1$) component. The IEEE Nordic test system has four area namely, 1) “North” with hydro generation and some load, 2) “Central” with much higher load and thermal power generation, 3) “Equiv” connected to the “North”, which includes a simple equivalent of an external system, and 4) “South” with thermal generation, which is rather loosely connected to the rest of the system. The IEEE Nordic test system is loaded in such a way that there are large transfers that flow from the North to Central areas. The Nordic test system experiences a long-term voltage instability phenomenon when a three-phase fault near bus 4032 is cleared by tripping of the line 4032-4044. The tripping of the line 4032-4044 causes additional load demand to flow through the remaining tie lines resulting in a sudden distribution side voltage drop that is corrected by the LTCs [21]. However, as described in detail in [21], after the disturbance the maximum power that can be delivered by combined generation and transmission system is smaller than what the LTCs attempt to restore resulting in voltage instability phenomenon [21] (*in the interest of space, the event is not fully explained in this initial draft but rather we refer to the work in [21] for more details about this event in Nordic power grid*). This instability phenomenon driven by OELs and LTCs takes place a few minutes after the initiating event is cleared as explained in detail in [21]. The plot of the dominant eigenvalue of the system versus time is shown in Fig. 8 demonstrating the onset of instability is around 63s. In this paper, we propose a method to identify the onset of a voltage emergency situation.

B. Characteristic curves to identify the maximum power point

In this subsection, first, we provide a simple three bus example to explain the working principle behind [18]. Second, using the same three bus example, we present the LD-VSI.

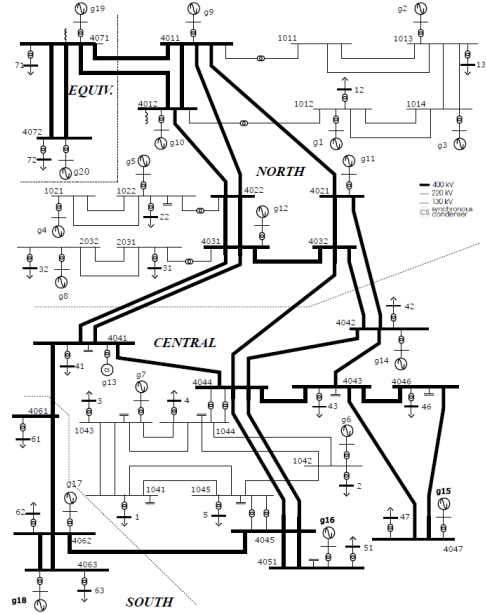


Fig. 6: One-line diagram of Nordic test system.

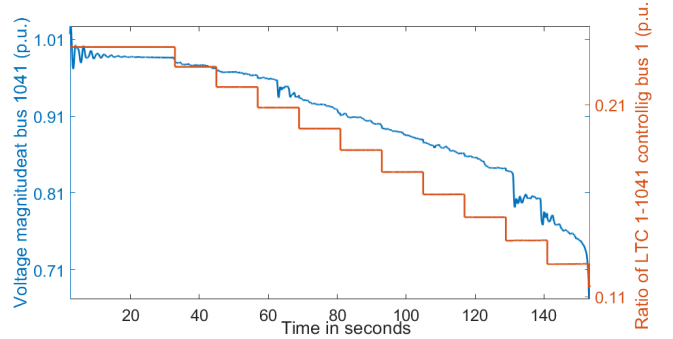


Fig. 7: Failed restoration of distribution voltage by LTC.

Let us consider the three bus fully connected network described in Section II. The loads at buses 2 (P_2) and 3 (P_3) are increased by increasing the λ from (1). As shown in Fig. 9, [18] proposed New LIVES Index (NLI) identify the nose point (maximum power point) by monitoring the sign change of the slope of the real power demand (P) versus load conductance (G) in the characteristic curve. As shown in Fig. 9, we propose a new decentralized VCPI known as local dynamic - voltage stability indicator (LD-VSI) to identify the nose point (maximum power point) by monitoring the sign change of the slope of the real power demand (P) versus the negative sign of LS-VSI ($-\Pi_1$) characteristic curve. This approach works as the LS-VSI monotonically reduces as λ increases. Thus, the change of sign of Π_2 from positive to negative corresponds to the maximum power point. In Fig. 9, it can be observed that both NLI [18] and the proposed index Π_2 identify the maximum power point at $\lambda = 7.09$ when their sign changes from positive to negative. Thus, LD-VSI (Π_2) can be used to identify voltage collapse driven by a large disturbance phenomenon. The proposed decentralized index at bus d to identify the maximum power point during a large disturbance LTVI phenomenon is given by

$$\text{LD-VSI} = \Pi_2|_{\text{at bus } d} = \frac{\Delta P_d}{-\Delta \Pi_1|_{\text{at bus } d}}, \quad (12)$$

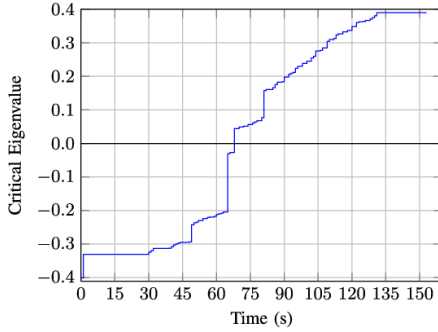


Fig. 8: Dominant eigenvalue for unstable scenario [18]. Zero crossing at 63s corresponds to onset of instability.

where Δ indicates the filtering method described in [18]. The overall procedure is described in Algorithm 2.

The key advantage of LD-VSI over NLI is that the slope transition is much more prominent for LD-VSI compared to NLI due to the fact that its denominator (LS-VSI) is within a smaller range (0 to 1) compared to the load conductance G (0 to 13). **The large range of G makes the slope (NLI) smaller and sensitive to perturbations due to noise. This issue is reduced in LD-VSI (Π_2) making it more robust to noise compared to NLI.** A further advantage is that the characteristic curve P vs Π_1 becomes nearly vertical as the system approaches the SNBP (maximum λ). This is because the value of LS-VSI (Π_1) approaches zero at the critical bus near the SNBP. **Thus, LD-VSI (Π_2) can also be used to identify the SNBP of the system and the critical bus when the value of Π_2 approaches a large negative value. This cannot be done by using the LIVES and New LIVES indices in [17], [18].** Furthermore, NLI can only be calculated when the load conductance increases at the bus of interest otherwise it discards the measurement data, this does not allow continuous monitoring of the grid. Whereas, the proposed LD-VSI does not have any such assumptions. Simulation discussion for LD-VSI is presented in Section VI.

Algorithm 2 Detection of onset of voltage collapse for large disturbance events: local monitoring of maximum power point

Input : Measurements: $\bar{V}_d, I_{d,k}, Y_{d,k} \forall k \in \mathcal{N}(d), \alpha_p, \beta_p, \gamma_p$ and $\alpha_q, \beta_q, \gamma_q$ at bus d , window length T .

Output: Alarm to indicate onset of voltage collapse.

- 1: Calculate Π_1 for all time steps in time window T ;
- 2: Calculate Δp_d and $\Delta \Pi_1|_{\text{at bus } d}$ using the filter in [18];
- 3: Calculate LD-VSI (Π_2) at bus d using (12);
- 4: **return** If $\Pi_2 < 0$ then trigger alarm.

V. SIMULATION 1 IN MATPOWER: SMALL DISTURBANCE LONG-TERM VOLTAGE STABILITY

The proposed Algorithm 1 is tested on IEEE 30-bus system [23] and 2000-bus Texas synthetic grid [24]. Similar results are observed for IEEE 300 and 2383-bus (Polish) systems as well. In the interest of space, the results for larger bus systems are not included. To obtain the voltage, current phasor measurements, and the true voltage stability margin, we used the non-divergent robust Newton-Raphson based power flow solver known as continuation power flow (CPF) from MATPOWER [20]. In this section, we show that the proposed decentralized LS-VSI in Algorithm 1 is advantageous com-

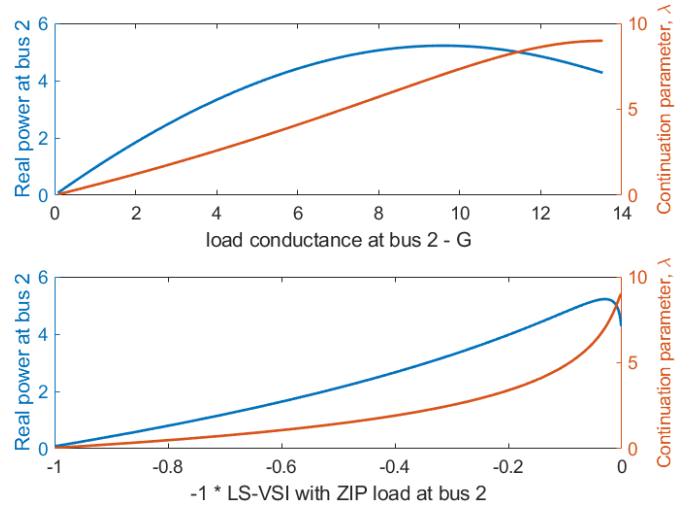


Fig. 9: Characteristic curves to monitor the maximum power point (nose point). (P_2 versus G_2) for [18], and (P_2 versus $-\Pi_1$) for proposed algorithm 2.

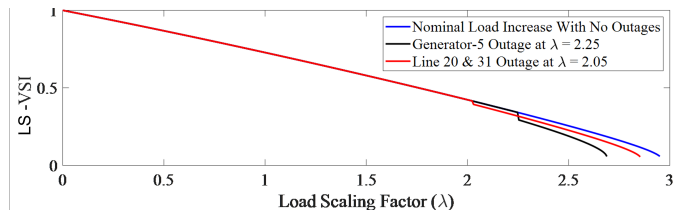


Fig. 10: Impact on LS-VSI at the monitored substation (bus 30) due to disturbances in unmonitored areas.

pared to both centralized and decentralized VCPIs. The LS-VSI is shown to be highly robust to noisy measurements when compared with other decentralized and centralized VCPIs. We also show that LS-VSI (11) can capture the impact of system disturbances that occur away from the monitored location. We also show that the proposed decentralized VSI can identify the critical bus SNBP accurately while [8] [19] fail.

A. Proposed decentralized LS-VSI versus decentralized and centralized VCPIs

In practice, there are specific regions of the power system that are critical for LTVI and can be identified by offline means. Thus, the system operator is interested in online LTVI monitoring at a few strategic locations/regions. For instance, in the IEEE-30 bus system, the operator would like to monitor the bus 30 (the critical bus [8]). To calculate centralized VCPIs [2] at bus 30, the voltage measurements at all the buses are required. To calculate the proposed LS-VSI at bus 30, the voltage measurements at bus 30 and adjacent branch current measurements are sufficient.

Tab. I compares the requirements of centralized VCPIs, a decentralized VCPI (LTI [5]), and the proposed LS-VSI to monitor bus 30 (the critical bus). **It can be observed from Tab. I that the proposed LS-VSI is robust to noise in field measurements (validated in Section V-C), requires only one device (for local measurement), and uses model information about adjacent branch admittances. The decentralized LTI [5] and centralized VCPIs [2] lack at least one of these desirable criteria.**

TABLE I: Comparison between centralized, proposed decentralized LS-VSI and other decentralized method to monitor the LTVI of any single substation in IEEE 30-bus system.

Monitoring Method	# Monitoring devices	Measurement noise robustness	Model info. req.
Centralized [2]	30	Robust	Full Y_{bus}
Decentralized LTI [5]	1	Not robust	No information
Proposed LS-VSI	1	Robust	Adjacent branch Y

B. Load increase with various system disturbances

In this subsection, we will demonstrate that the proposed LS-VSI can identify the maximum system loading and can also capture the impact of line outages & generator outages that are not in the immediate neighborhood of the monitored bus. Three loading scenarios are considered

- 1) Nominal load increase where all loads and generators are increased in proportion to their base value.
- 2) Load increase with line 20 & line 31 outaged at $\lambda = 2.05$.
- 3) Load increase with generator-5 outage at $\lambda = 2.25$.

CPF in MATPOWER is used to simulate the system at increasing load levels (using continuation parameter λ) and the voltage/currents are used to calculate the proposed LS-VSI. Fig. 10 shows the plot of LS-VSI at bus 30 for the above-mentioned three scenarios versus the load scaling factor (λ) compared to the base case loading condition ($\lambda = 1$). As per the derivation in Section III-B, we expect the LS-VSI to be near 1 at no-load and monotonically decrease to 0 at the SNBP. This pattern is indeed observed in all the scenarios validating the proposed method for monitoring LTVI. Further, the outages in the above scenarios (2) and (3) are not in the neighborhood of bus 30 but their impact *is captured by the bus voltage and branch currents (measurements at bus 30) which in turn causes a sudden drop in the value of proposed LS-VSI* when the outages occur. Additionally, Fig. 10 shows that the drop in the proposed decentralized LS-VSI implies that an event leading to lesser loading capacity has occurred and this fact can be used to trigger mitigation controls locally.

The behavior of the LS-VSI has a similar behavior for other scenarios such as different load increase direction, generator VAR limits, and capacitor switching. **Thus, the proposed index can monitor the system stability with system disturbances that are not directly in the monitored bus vicinity, making this method applicable for practical systems.**

C. Impact of noisy measurements on decentralized LS-VSI, Thevenin-based decentralized and centralized VCPIs

In this subsection, we compared the proposed local LS-VSI with other methods when there is noise in the field measurements. We show that LS-VSI is robust to noisy measurements when compared with local Thevenin index (LTI) [5] and a centralized Thevenin index (CTI) [2]. LTI [5] uses only local measurements to calculate its index while CTI [2] uses full state and full system admittance matrix to calculate its index.

To understand the impact of noise on the proposed methodology, an additive Gaussian noise with zero mean and standard deviation of 0.001 p.u. on voltage magnitude (σV_m), 0.01° , 0.05° , 0.5° on phase angles (σV_a) are introduced in the measurements according to the analysis of field-tested

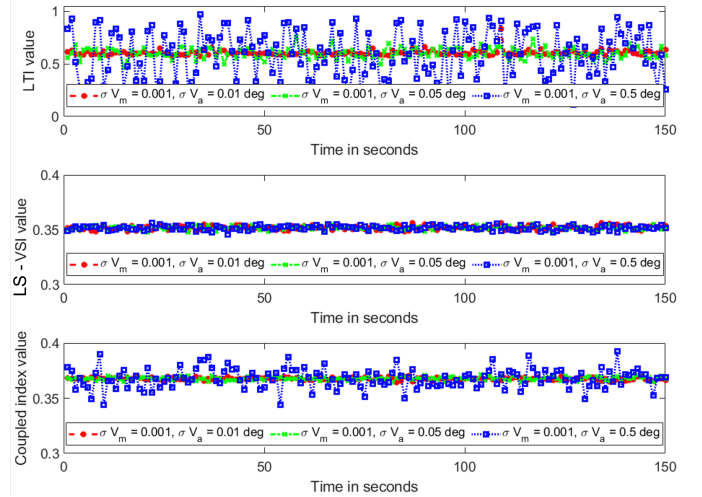


Fig. 11: Effect of noisy data on proposed and other methods.

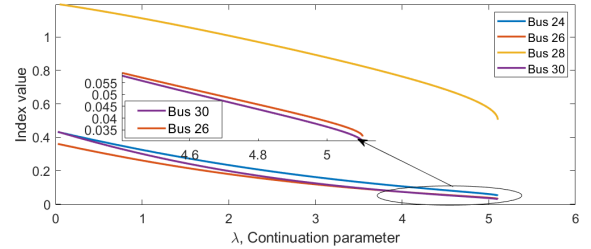


Fig. 12: Proposed decentralized LS-VSI at different buses in the network. Bus 30 has smallest value.

PMUs by New England ISO [25], [26] and IEEE standard for acceptable PMU errors [27]. As shown in Fig. 11, using the noisy measurements, the LTI, CTI, and the proposed LS-VSI are calculated at bus 30. Since all indices lie between 0 and 1, their variance can be compared and used to quantify the robustness of each method to measurement noise. It can be observed from the plots that the variability of the proposed LS-VSI and CTI is much smaller than LTI. Furthermore, the LS-VSI is comparable to that of the CTI, which uses information on the full system state and model information. Tab. II presents the standard deviation of the indices due to noise in the field measurements. **Thus, the robustness of the LS-VSI to noisy measurements is better than LTI and is comparable to CTI while needing only local measurements and local system information.**

TABLE II: The standard deviation (σ) for the LS-VSI, LTI and CTI at bus 30 in IEEE-30 bus system when Gaussian noise is introduced in the measurements ($\sigma V_m = 0.001$ p.u.).

Noise levels	Proposed LS-VSI	LTI [5]	CTI [2]
$\sigma V_a = 0.01^\circ$, [27]	$\sigma = 0.001$	$\sigma = 0.02$	$\sigma = 0.001$
$\sigma V_a = 0.05^\circ$, [25]	$\sigma = 0.002$	$\sigma = 0.05$	$\sigma = 0.002$
$\sigma V_a = 0.5^\circ$, [25]	$\sigma = 0.003$	$\sigma = 0.2$	$\sigma = 0.008$

D. Identification of critical bus of a system with ZIP loads using proposed decentralized LS-VSI and D-VSI from [8]

In this subsection, we present the results of the proposed decentralized LS-VSI and distributed index (D-VSI) from [8]. The experiment is conducted on IEEE 30 bus system with system wide ZIP loads whose Z, I, P compositions of real and reactive load powers are $\alpha_p = \alpha_q = 0.9$, $\beta_p = \beta_q = 0$, $\gamma_p = \gamma_q = 0.1$ respectively.

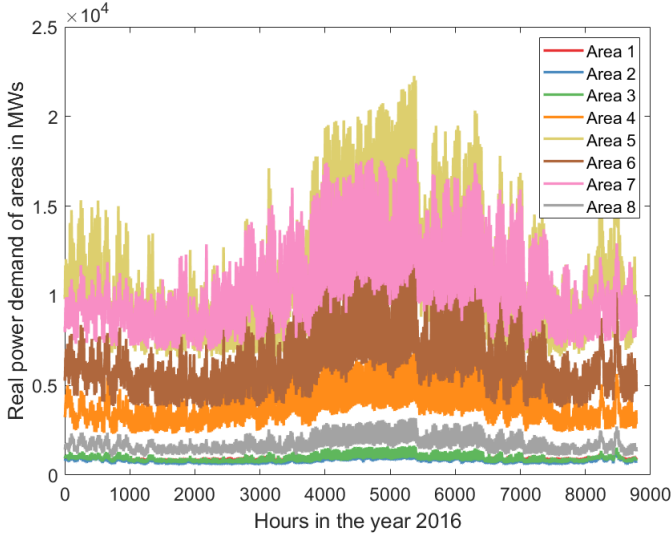


Fig. 13: Load profiles of eight different areas in Texas synthetic grid for the year 2016.

The PV curve is traced by using the CPF solver from MATPOWER [20]. As detailed in Section II, the SNBP does not occur at the maximum power anymore due to the presence of the ZIP load models in the network. The SNBP occurs when the continuation parameter $\lambda = 5.1$. Since we know that bus 30 is the critical bus that induces LTVI. When $\lambda = 5.1$, the index value at bus 30 must be the least value when compared to index values at other buses in the network indicating that bus 30 is the critical bus. **However, [8] incorrectly identifies the critical bus to be bus 26. This is because of its incorrect assumption of system-wide constant power loads. Whereas the proposed LS-VSI correctly identifies the critical bus as bus 30 as shown in Fig. 12.**

E. Texas synthetic grid: stressing the sinks in Coast area

In this subsection, we present the results of LS-VSI implemented on the Texas synthetic 2000-bus system [24], [28], [29]. The Texas synthetic grid is divided into eight areas with four different voltages levels like 500 kV, 230 kV, 161 kV, and 115 kV. Fig. 13 presents the load profiles of the eight areas that are designed in a realistic manner for the year 2016 by [30], [31]. It can be observed that the area with the greatest demand is area 5 corresponds to the Coast area [24].

It is a standard practice to study the voltage stability phenomenon for large interconnected grids by stressing the area of concern and observing the imports and exports between the areas as discussed in [32], [33]. Here, the loads in area 5 are increased linearly using the CPF from MATPOWER [20]. Fig. 14 shows the PV curves at different buses, and bus 7095 (critical bus) located in area 7 has the lowest voltage magnitude among all buses in the system when voltage collapse occurs.

It can be observed that the voltage magnitude of the critical bus is 0.94 p.u. when voltage collapse occurs. This is because the practical grids are designed to maintain voltages within a range of 0.9 to 1.1 p.u. for a large set of operating conditions and loading [34]. Therefore, using the voltage magnitude as a signal to trigger local measurement-based SPSs is not always straightforward as it is not a good indicator of system stress.

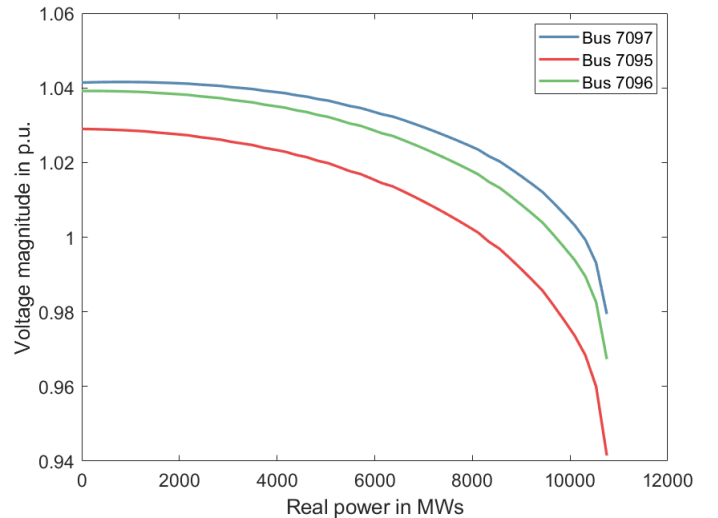


Fig. 14: PV curves at different buses when the loads in area 5 are increased linearly.

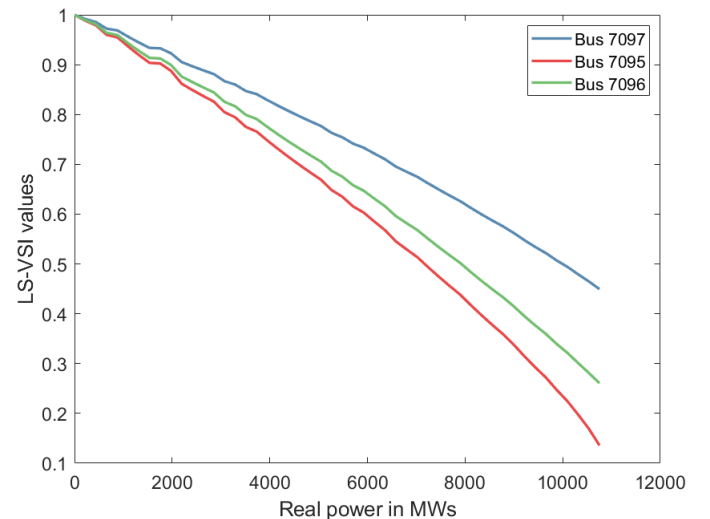


Fig. 15: LS-VSI values at different local buses to identify the LTVI phenomenon.

In contrast, the LS-VSI of bus 7095 shown in Fig. 15 becomes close to zero, indicating a high risk of voltage collapse. **Thus, LS-VSI values can be computed in real-time by using the local measurements, which are helpful to trigger local measurement-based SPSs reliably.**

VI. SIMULATION 2 IN PSSE: LARGE DISTURBANCE LONG-TERM VOLTAGE STABILITY

In this section, the proposed index (LD-VSI) is validated and compared with NLI [18] for large disturbance long-term voltage instability in the Nordic system. The IEEE Nordic system is operated in the unstable scenario described in Section IV-A and simulated in PSSE dynamic simulator. This scenario is explained more in detail (as operating point A) in [21]. To evaluate the impact of measurement noise on LD-VSI, an additive Gaussian noise with zero mean and standard deviation of 0.001 p.u. on voltage magnitude ($\sigma V_m = 0.001 p.u.$), 0.5° on phase angles ($\sigma V_a = 0.5^\circ$) are introduced according to the analysis of field-tested PMUs by New England ISO [25], [26] and IEEE standard for acceptable PMU errors [27]. To demonstrate the robustness of the proposed LD-VSI with

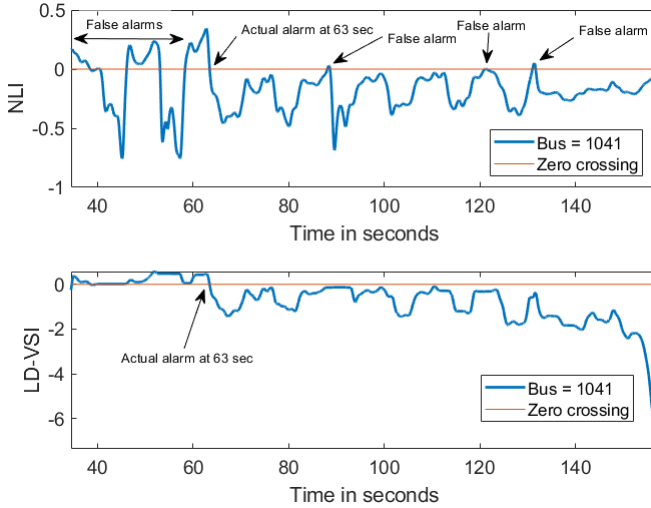


Fig. 16: Comparison of NLI [18] and proposed LD-VSI.

regard to noise, it is compared with the NLI method [18] and results are presented in Fig. 16. Both NLI and LD-VSI methods use the same moving average filter to mitigate the impact of noisy measurements as described in the reference [18]. The expected behaviors of LD-VSI and NLI are that they both transition from positive to negative during a voltage emergency situation as explained in Section IV-B and Fig. 9.

As shown in Fig. 16 both NLI and LD-VSI correctly identify the voltage emergency situation at 63s but NLI is observed to be noisier. For example, between 40s and 60s, NLI triggers false alarms at 40s and 55s. However, LD-VSI does not trigger such false alarms before correctly identifying the voltage emergency situation correctly at 63s. This robustness to noise makes it easier for the operator to reliably implement and identify the voltage emergency situations without having to determine the optimal value for the filter window size (hyperparameter) when compared to the NLI method. Furthermore, after 80s, NLI again swings between positive and negative values creating false alarms. However, that is not the case with the LD-VSI. Finally, it can be seen that the LD-VSI becomes more negative as the system approaches collapse around 160s. This can also be used by any mitigation scheme to alleviate system stress. This feature is not observed in the NLI as its value does not vary significantly as the system approaches SNBP. **Thus, the robustness of the proposed LD-VSI, its smaller filter window size, and its behavior as the system approaches SNBP make it more favorable to use in comparison with similar methods like [17], [18].**

VII. CONCLUSION

This paper proposes two local measurement based voltage stability indices that can monitor long-term voltage instability occurring over various time scales. The key novelty of the first index (LS-VSI) lies in its decentralized nature, ability to incorporate ZIP loads, and robustness to measurement noise. LS-VSI monitors LTVI by recasting the power flow equations as circles and exploiting the relation between the SNBP and the intersection points. LS-VSI can identify LTVI in scenarios with non-local line trips, generator outages, VAR limits, and shunt capacitor switching. It is shown that the power flow equation-based approach of the proposed decentralized LS-VSI makes it robust to measurement noise which

adversely affects the other decentralized techniques such as local Thevenin methods. It is also shown that the LS-VSI is a good indicator to identify voltage collapse and reliably trigger local measurement-based SPSs. LS-VSI is compared with a centralized method and is shown to be comparably robust to measurement noise while requiring lesser measurement infrastructure and system information, making it attractive for practical implementation.

Next, we utilized the properties of LS-VSI to develop the second local index (LD-VSI) for identifying the onset of voltage instability due to large disturbances. We demonstrated the advantage of the proposed LD-VSI over the state-of-the-art method on the Nordic test system through dynamic simulations in PSSE. It is observed that the LD-VSI is more robust to measurement noise and can also distinguish between SNBP and maximum power point, making it a superior method to comparable methods in the literature.

REFERENCES

- [1] T. Van Cutsem and C. Vournas, "Voltage stability analysis of electric power systems," *Springer Science & Business Media*, 1998.
- [2] Y. Wang, I. R. Pordanjani, W. Li, W. Xu, T. Chen, E. Vaahedi, and J. Gurney, "Voltage stability monitoring based on the concept of coupled single-port circuit," *IEEE Trans. on Power Systems*, 2011.
- [3] Y. Weng, R. Rajagopal, and B. Zhang, "A geometric analysis of power system loadability regions," *IEEE Trans. on Smart Grid*, 2019.
- [4] F. Gubina and B. Strmcnik, "Voltage collapse proximity index determination using voltage phasors approach," *IEEE Trans. on Power Systems*, 1995.
- [5] K. Vu, M. M. Begovic, D. Novosel, and M. M. Saha, "Use of local measurements to estimate voltage-stability margin," *IEEE Trans. on Power Systems*, 1999.
- [6] B. Milosevic and M. Begovic, "Voltage-stability protection and control using a wide-area network of phasor measurements," *IEEE Trans. on Power Systems*, 2003.
- [7] G. Verbic and F. Gubina, "A new concept of voltage-collapse protection based on local phasors," *IEEE Trans. on Power Delivery*, 2004.
- [8] K. P. Guddanti, A. R. R. Matavalam, and Y. Weng, "PMU-based distributed non-iterative algorithm for real-time voltage stability monitoring," *IEEE Trans. on Smart Grid*, 2020.
- [9] M. Glavic and T. Van Cutsem, "A short survey of methods for voltage instability detection," in *IEEE Power and Energy Society General Meeting*, 2011.
- [10] T. Van Cutsem and C. Vournas, "Emergency voltage stability controls: an overview," in *IEEE Power Engineering Society General Meeting*, 2007.
- [11] C. Barbier and J. P. Barret, "An analysis of phenomena of voltage collapse on a transmission system," *Revue Générale d'Electricité*, 1980.
- [12] M. K. Pal, "Voltage stability conditions considering load characteristics," *IEEE Trans. on Power Systems*, 1992.
- [13] C. Concordia and S. Ihara, "Load representation in power system stability studies," *IEEE Trans. on Power Apparatus and Systems*, 1982.
- [14] T. J. Overbye, "Effects of load modelling on analysis of power system voltage stability," *International Journal of Electrical Power & Energy Systems*, 1994.
- [15] P. Kundur, J. Paserba, V. Ajjarapu, G. Andersson, A. Bose, C. Canizares, N. Hatziaargyriou, D. Hill, A. Stankovic, C. Taylor *et al.*, "Definition and classification of power system stability IEEE/Cigre joint task force on stability terms and definitions," *IEEE Trans. on Power Systems*, 2004.
- [16] N. Hatziaargyriou, J. Milanovic, C. Rahmann, V. Ajjarapu, C. Canizares, I. Erlich, D. Hill, I. Hiskens, I. Kamwa, B. Pal *et al.*, "Definition and classification of power system stability revisited & extended," *IEEE Trans. on Power Systems*, 2020.
- [17] C. D. Vournas and T. Van Cutsem, "Local identification of voltage emergency situations," *IEEE Trans. on Power Systems*, 2008.
- [18] C. D. Vournas, C. Lambrou, and P. Mandoulidis, "Voltage stability monitoring from a transmission bus pmu," *IEEE Trans. on Power Systems*, 2016.
- [19] J. W. Simpson-Porco and F. Bullo, "Distributed monitoring of voltage collapse sensitivity indices," *IEEE Trans. on Smart Grid*, 2016.
- [20] R. D. Zimmerman, C. E. Murillo-Sánchez, R. J. Thomas *et al.*, "Matpower: Steady-state operations, planning, and analysis tools for power systems research and education," *IEEE Trans. on power systems*, 2011.

- [21] T. Van Cutsem, M. Glavic, W. Rosehart, C. Canizares, M. Kanatas, L. Lima, F. Milano, L. Papangelis, R. A. Ramos, J. A. dos Santos *et al.*, "Test systems for voltage stability studies," *IEEE Trans. on Power Systems*, 2020.
- [22] "Benchmark systems for voltage stability, nordic test system," *IEEE Power & Energy Society, Power Syst. Dyn. Performance Committee*, 2016. [Online]. Available: <https://cmte.ieee.org/pes-psdp/489-2/>
- [23] R. D. Christie, *IEEE-30 Bus system description*, 1993. [Online]. Available: labs.ece.uw.edu/pstca/pf30/pg_tca30bus.htm
- [24] A. B. Birchfield, T. Xu, K. M. Gegner, K. S. Shetye, and T. J. Overbye, "Grid structural characteristics as validation criteria for synthetic networks," *IEEE Trans. on Power Systems*, 2017.
- [25] Q. Zhang, X. Luo, D. Bertagnolli, S. Maslennikov, and B. Nubile, "PMU data validation at ISO New England," in *IEEE Power & Energy Society General Meeting*, 2013.
- [26] M. Brown, M. Biswal, S. Brahma, S. J. Ranade, and H. Cao, "Characterizing and quantifying noise in PMU data," in *IEEE Power and Energy Society General Meeting*, 2016.
- [27] K. E. Martin, "Synchrophasor measurements under the IEEE standard C37.118.1-2011 with amendment C37.118.1 a," *IEEE Trans. on Power Delivery*, 2015.
- [28] A. B. Birchfield, K. M. Gegner, T. Xu, K. S. Shetye, and T. J. Overbye, "Statistical considerations in the creation of realistic synthetic power grids for geomagnetic disturbance studies," *IEEE Trans. on Power Systems*, 2017.
- [29] K. M. Gegner, A. B. Birchfield, T. Xu, K. S. Shetye, and T. J. Overbye, "A methodology for the creation of geographically realistic synthetic power flow models," in *IEEE Power and Energy Conference at Illinois (PECI)*, 2016.
- [30] H. Li, A. L. Bornsheuer, T. Xu, A. B. Birchfield, and T. J. Overbye, "Load modeling in synthetic electric grids," in *IEEE Texas Power and Energy Conference*, 2018.
- [31] H. Li, J. H. Yeo, A. L. Bornsheuer, and T. J. Overbye, "The creation and validation of load time series for synthetic electric power systems," *IEEE Trans. on Power Systems*, 2021.
- [32] B. Sapkota and V. Vittal, "Study of voltage collapse cases of a large power system using static and dynamic approaches," in *IEEE/PES Power Systems Conference and Exposition*, 2009.
- [33] M. Randhawa, B. Sapkota, V. Vittal, S. Kolluri, and S. Mandal, "Voltage stability assessment of a large power system," in *IEEE PES General Meeting - Conversion and Delivery of Electrical Energy in the 21st Century*, 2008.
- [34] A. B. Birchfield, T. Xu, and T. J. Overbye, "Power flow convergence and reactive power planning in the creation of large synthetic grids," *IEEE Trans. on Power Systems*, 2018.